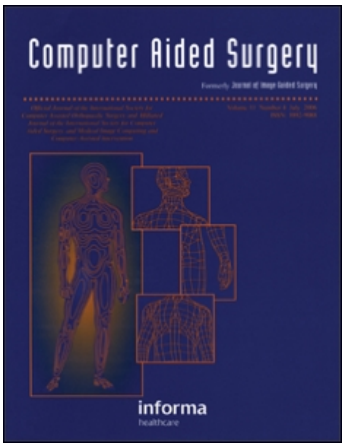

Computer Aided Surgery
Publication details, including instructions for authors and subscription information:
http://www.informaworld.com/smpp/title~content=t713723590

Robot-assisted needle placement in open MRI: System architecture, integration and validation

S. P. DiMaio [a]; S. Pieper [b]; K. Chinzei [c]; N. Hata [a]; S. J. Haker [a]; D. F. Kacher [a]; G. Fichtinger [d]; C. M. Tempany [a]; R. Kikinis [a]
[a] Brigham and Women's Hospital, Harvard Medical School, Boston, Massachusetts, USA [b] Isomics, Inc., Cambridge, Massachusetts, USA [c] National Institute of Advanced Industrial Science and Technology (AIST), Tsukuba, Japan [d] Johns Hopkins University, Baltimore, Maryland, USA

Online Publication Date: 01 January 2007

To cite this Article DiMaio, S. P., Pieper, S., Chinzei, K., Hata, N., Haker, S. J., Kacher, D. F., Fichtinger, G., Tempany, C. M. and Kikinis, R.(2007)'Robot-assisted needle placement in open MRI: System architecture, integration and validation',Computer Aided Surgery,12:1,15 — 24

To link to this Article: DOI: 10.1080/10929080601168254

URL: http://dx.doi.org/10.1080/10929080601168254

Computer Aided Surgery, January 2007; 12(1): 15–24

informa
healthcare

BIOMEDICAL PAPER

Robot-assisted needle placement in open MRI: System architecture, integration and validation

S. P. DIMAIO[1], S. PIEPER[2], K. CHINZEI[3], N. HATA[1], S. J. HAKER[1], D. F. KACHER[1], G. FICHTINGER[4], C. M. TEMPANY[1], & R. KIKINIS[1]

[1]*Brigham and Women's Hospital, Harvard Medical School, Boston, Massachusetts,* [2]*Isomics, Inc., Cambridge, Massachusetts, USA,* [3]*National Institute of Advanced Industrial Science and Technology (AIST), Tsukuba, Japan, and* [4]*Johns Hopkins University, Baltimore, Maryland, USA*

(Received 1 May 2006; accepted 23 August 2006)

Abstract

In prostate cancer treatment, there is a move toward targeted interventions for biopsy and therapy, which has precipitated the need for precise image-guided methods for needle placement. This paper describes an integrated system for planning and performing percutaneous procedures with robotic assistance under MRI guidance. A graphical planning interface allows the physician to specify the set of desired needle trajectories, based on anatomical structures and lesions observed in the patient's registered pre-operative and pre-procedural MR images, immediately prior to the intervention in an open-bore MRI scanner. All image-space coordinates are automatically computed, and are used to position a needle guide by means of an MRI-compatible robotic manipulator, thus avoiding the limitations of the traditional fixed needle template. Automatic alignment of real-time intra-operative images aids visualization of the needle as it is manually inserted through the guide. Results from in-scanner phantom experiments are provided.

Keywords: *Prostate cancer, percutaneous therapy, targeted needle biopsy, open MRI, robotic assistant, MRI-compatible robot*

Introduction

Current therapies for the treatment of prostate cancer, such as radical prostatectomy or external beam radiation, are directed at the entire prostate. Newer approaches are beginning to become more focal or targeted, as can be seen with intensity-modulated radiation therapy (IMRT), dose-escalated brachytherapy, and focal cryotherapy. There are two major drivers for this trend, namely the rapidly increasing incidence of the disease (expected to double by 2015) and its low mortality (4-8%). Accurate navigation for the targeting of surgical instruments (e.g., biopsy and therapy needles), based on pre-operative trajectory plans and intra-operative guidance, is a challenging problem in image-guided therapy. MRI is an attractive choice for guiding needles to targets within the prostate due to its excellent soft tissue contrast, multi-parametric imaging protocols, high spatial resolution, and multiplanar volumetric imaging capabilities. The peripheral zone (PZ) can be seen in T2-weighted images and used to identify suspicious nodules. A multi-year clinical trial of MRI-guided prostate biopsy using an intra-operative open 0.5T MR imaging system (GE Signa SP) is described in reference [1].

In the last few years, a number of promising new multi-parametric imaging methods have emerged for detection of tumors in the prostate, including proton spectroscopy (MRSI), quantitative mapping of T2, dynamic intravenous gadolinium-enhanced MR, and apparent diffusion coefficient (ADC) [2–6]. Clinical studies are beginning to show

Correspondence: Simon DiMaio, Ph.D., Surgical Planning Laboratory, Department of Radiology, Brigham and Women's Hospital, Harvard Medical School, Boston, MA 02115, USA. E-mail: simond@bwh.harvard.edu

Part of this research was previously presented at the 14th Annual Medicine Meets Virtual Reality Conference (MMVR14) held in Long Beach, California, in January 2006.

ISSN 1092–9088 print/ISSN 1097–0150 online © 2007 Informa UK Ltd.
DOI: 10.1080/10929080601168254

clear benefits for targeted approaches based on such image information in the detection and treatment of prostate cancer [7]. However, current clinical practice is still limited in its ability to reliably target needles within small soft-tissue targets on the order of 5 mm or less. Stereotactic frames and needle template guides are typically used to calibrate and constrain instrument motion, but often lead to inflexible guidance mechanisms and workflows. This paper introduces a system that integrates an interactive planning system and real-time imaging control interface with an MRI-compatible robotic assistant that acts as a dynamic needle guide for precise, yet flexible, targeted needle placement. Our clinical model is based on needle biopsy and prostate brachytherapy procedures that are currently performed under MRI guidance at the Brigham and Women's Hospital (BWH) in Boston [8]. These procedures employ a needle template that is very similar to that used in transrectal ultrasound (TRUS)-guided brachytherapy – a fixed guide consisting of a grid of holes spaced 5 mm apart, through which needles are inserted. The robotic system that has been developed in this work eliminates the constraints imposed by the template on trajectory resolution and needle orientation by providing a dynamic computer-controlled needle guide [9]. The system has been validated in phantom experiments and approved for a clinical trial in a transperineal prostate biopsy procedure.

The remainder of this section describes the clinical relevance of targeted needle placement and prior work related to robot-assisted needle placement with MRI guidance. The *Materials and methods* section describes the architecture of the robot-assisted system, which includes a planning interface and an MRI-compatible needle-positioning device, along with issues of calibration and control. This is followed by preliminary results from in-scanner phantom tests. Finally, conclusions and scope for future work are discussed.

Clinical relevance

One out of every six men in the United States will be diagnosed with prostate cancer at some point in his life [10]. The definitive method of diagnosis is core needle biopsy, and each year approximately 1.5 million core needle biopsies are performed, yielding approximately 220,000 new prostate cancer cases [10]. If the cancer is found to be confined to the prostate, then low-dose-rate permanent brachytherapy, performed by implanting a large number (50–150) of radioactive pellets/seeds into the prostate using thin needles (typically 18G), is a common treatment option [11]. A complex seed distribution pattern must be achieved with great accuracy in order to eradicate the cancer while minimizing radiation toxicity to adjacent healthy tissues. Over 40,000 brachytherapies are performed in the US each year, and the number is steadily growing [12]. Transrectal Ultrasound (TRUS) is the current ''gold standard'' for guiding both biopsy and brachytherapy due to its fast image acquisition rate, low cost, and apparent ease of use [13]. However, current TRUS-guided biopsy has a detection rate of 20-30% [14]. Furthermore, in TRUS-guided brachytherapy the implant procedure cannot be effectively monitored, as implanted seeds cannot easily be seen in the images. MRI seems to possess many of the capabilities that TRUS is lacking: It has high sensitivity for detecting prostate tumors, high spatial resolution, excellent soft tissue contrast, and multiplanar volumetric imaging capabilities [15]. Furthermore, MR image registration techniques [16] allow images obtained before the day of the procedure to be used for intra-procedural targeting and planning. Therefore, MR imaging techniques that are sensitive to cancer but too time-consuming for intra-operative use, such as diffusion imaging [16] and spectroscopic studies [2, 5], as well as derived images designed to enhance specificity [17] or to incorporate knowledge of the most likely locations of tumors within the gland [18], can be used to full effect. The clinical efficacy of MRI-guided prostate brachytherapy and biopsy was demonstrated by D'Amico, Tempany and colleagues at BWH using a 0.5T open-MRI scanner to plan and monitor transperineal needle placement [8, 19]. The needles were inserted manually using a plastic guide comprising a grid of holes, with the patient oriented in the lithotomy position, similarly to the TRUS-guided approach. Zangos et al. used a transgluteal approach with 0.2T MRI, but did not specifically target the tumor foci [20], while Susil et al. described four cases of transperineal prostate biopsy in a closed-bore scanner, where the patient was moved out of the bore for needle insertions and then placed back in the bore to confirm satisfactory placement [21]. Beyersdorff et al. performed targeted transrectal biopsy in a 1.5T MRI unit with a passive articulated needle guide and have reported 12 cases of biopsy to date [22].

Needle misplacement

To the best of our knowledge, the accuracy of needle placement in transperineal prostate interventions has never been formally and quantitatively evaluated. Determining the accuracy of needle placement within the targeted tissue is difficult

using current forms of navigation and guidance techniques. We have conducted a number of preliminary studies to investigate the accuracy of needle placement during MRI-guided transperineal prostate biopsy at BWH. From this, a taxonomy of factors that contribute to lower-than-desired accuracy is being developed. In a retrospective analysis of 10 clinical cases, we measured the distances between the pre-planned targeted locations and the actual needle tip visible in Fast Gradient Recalled (FGR) MR images acquired intra-operatively. 18-gauge core biopsy needles were used in these cases. The mean distance between the pre-planned locations and the actual measured needle tip coordinates for all biopsy locations was found to be 6.5 mm [23].

These preliminary experiments indicate that, despite advances in image guidance and navigation systems, needle placement accuracy is still too low to enable reliable targeting of tissue targets smaller than 5 mm in diameter due to uncertainties introduced by misregistration, overly constraining needle templates, needle deflection, and tissue motion [23].

Robot-assisted needle placement with MRI guidance

Robotic assistance has been investigated for guiding surgical instruments in MRI, beginning with neurosurgery [24] and then turning to percutaneous interventions [25,26]. Chinzei et al. developed a general-purpose robotic assistant for open MRI [27], and Krieger et al. presented a 2-DOF passive, un-encoded and manually manipulated mechanical linkage to aim a needle guide for transrectal prostate biopsy with MRI guidance [28]. This device was visually servoed into position, using three active tracking coils, then the patient was moved out of the scanner for needle insertion. Other recent developments in MRI-compatible mechanisms include haptic interfaces for fMRI [29] and multi-modality actuators and robotics [30].

Materials and methods

System architecture

The architecture of the MR-guided, robot-assisted percutaneous intervention system is shown in Figure 1. The three major subsystems, namely the planning environment, the MR scanner (GE Signa SP, Milwaukee, WI), and the motion-controlled robotic manipulator, are integrated as shown. The workflow is as follows:

1. Register pre-operative 1.5T MR images with pre-procedural 0.5T images I_{MRI}.
2. Visualize the fused dataset and specify a set of biopsy targets. Image visualization and target planning are performed using the 3D Slicer (http://www.slicer.org) [31]. For each biopsy plan, the

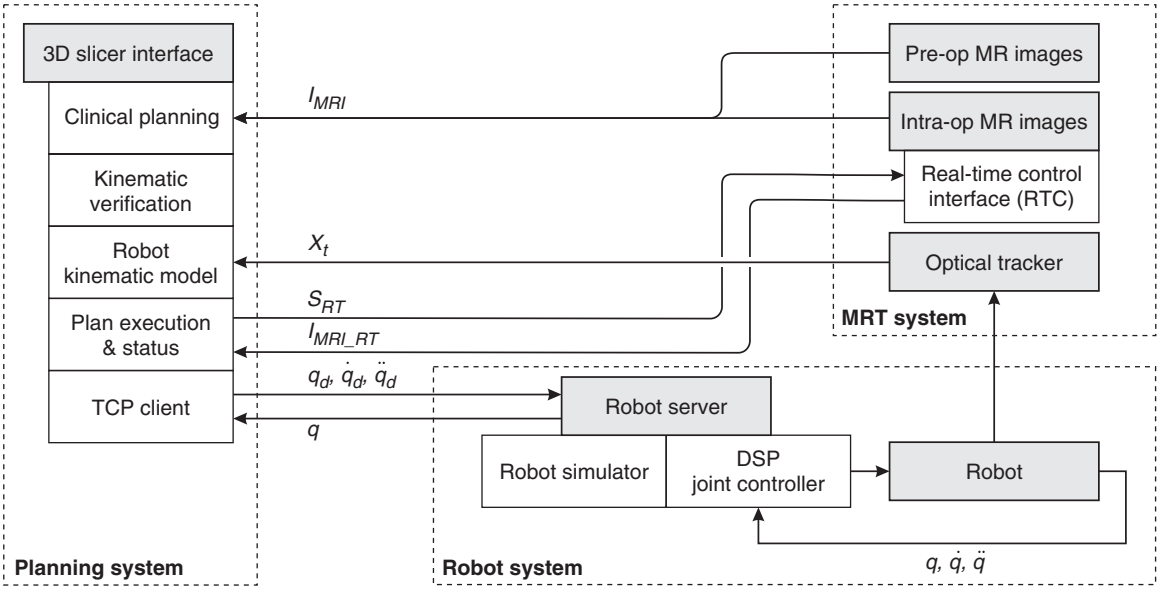

Figure 1. The percutaneous intervention system, comprising a planning sub-system, the MRT, and an MR-compatible robot.

physician specifies two points along the needle trajectory, namely a target and an entry point, by clicking directly on the images viewed in the 3D Slicer.
3. The robot is visualized in conjunction with the images and the biopsy plan, and positioning motions can be simulated and rendered on-screen for trajectory verification.
4. Calibrate robot to image space using a FlashPoint® optical tracking system.
5. Execute robot joint-space motion commands ($q, \dot{q}, \ddot{q}$) via an ethernet connection with the robot controller.
6. Robot motion proceeds and is continuously monitored and compared against a simulated robot motion model; any significant trajectory deviation halts motion.
7. Verify robot position by comparing the optically tracked needle guide position (X_t) with the biopsy plan. Steps 4-6 are repeated until the positioning error is satisfactorily compensated.
8. Imaging plane coordinates (S_{RT}) corresponding to the plane of the needle are sent from the 3D Slicer to the scanner's Real Time Control interface, and real-time images (I_{MRI_RT}) are acquired and displayed.
9. The needle is manually inserted through the needle guide, under real-time MR guidance (3-6s image update), and a biopsy sample is taken. Steps 4-8 are repeated until all target sites have been sampled.

Planning and needle targeting

This section describes image-based planning and interventional guidance methods that will be used during robot-assisted needle biopsy, based on current practice during open-MRI-guided prostate biopsy procedures at BWH. Prostate MRI at high field strengths, especially with combined endorectal and phased-array coils, provides images of high resolution and is used in prostate cancer staging as well as in the determination of extraprostatic disease. The T1- and T2-weighted images help to differentiate between post-biopsy hemorrhage and prostate cancer, which presents as a low T1 and low T2 lesion, while hemorrhage presents as a high T1 and low T2 lesion. Prior to MRI-guided prostate interventions, the information from pre-operative and pre-procedural images is registered, and target lesions are identified by a radiologist. Pre-operative and pre-procedural images are acquired in 1.5T closed-bore and 0.5T open-bore MR systems, respectively. A major difficulty in registration comes from the shape changes that can occur in soft tissues between imaging sessions. Such a shape change may, for example, be the result of changes in patient position necessitated by the procedures (the patient lies supine in the closed-bore MRI scanner, but in the lithotomy position within the open-bore scanner). A non-rigid registration method models basic biomechanical properties of soft tissue [16], and involves the following steps: (1) A 3D tetrahedral model of the entire prostate is created from segmented pre-operative 1.5T images; (2) the boundary surface of the capsule is extracted from this tetrahedral mesh and is registered to a corresponding capsule surface obtained from intra-operative images; (3) the surface point matches from step 2 are used as boundary conditions when solving a finite-element-based system of equations which models the volumetric deformation field within the gland; and (4) the volumetric deformation field from step 3 is used to interpolate pre-operative imaging data.

Once targets are identified and the biopsy procedure begins, we can provide the physician with feedback on the position of the needle relative to the targets. Real-time 2D FGR images of the prostate obtained throughout the biopsy procedure (3-second update rate) allow visualization of the prostate gland, rectum, bladder, catheter and needle position. However, these FGR images do not provide adequate contrast for visualization of sub-structures of the gland, namely the peripheral zone (PZ) and suspicious targets. These sub-structures are critical for precise biopsy sampling, and are provided by T2W images obtained before the procedure begins. The 3D Slicer effectively enables direct T2W visualization of the peripheral zone of the prostate with real-time FGR imaging visualized in the same frame of reference. Alternating views of the most recent real-time FGR and resampled T2W images are presented on a monitor in the bore of the scanner, with a delay of 1–2 seconds between the alternating images. In this way, the radiologist may see the needle artifact and its position relative to the PZ and suspicious foci, as shown in Figure 2, in order to verify needle placement.

MRI-compatible robotic needle guide

For this work, we use a first-generation MRI-compatible robotic assistant developed by Chinzei and colleagues [27,32,33] for use in a Magnetic Resonance Therapy operating room (MRT) equipped with a GE Signa SP open-MRI scanner. The robotic device consists of five linear motion stages arranged to form a 2-DOF orienting mechanism attached to a 3-DOF Cartesian positioning mechanism. The base of the robot is mounted above the surgeon's head in the open MRI magnet and two rigid arms reach down into the surgical field. The ends of the arms are linked to form a tool holder, which in this case is a linear needle guide (Figure 3(b)). There is a FlashPoint® optical marker attached to the needle guide, providing independent redundant encoding of end-effector pose, as shown in Figure 3(b-inset).

The mechanism is constructed almost entirely from non-ferrous, MR-compatible materials. The gantry frame is composed of aluminum and titanium elements, and each linear motion stage comprises plastic, titanium, stainless steel (YHD50) and beryllium-copper (Be-Cu) components. All sensors are optical and signals are transferred to and from the magnet room via fiber optics. Linear optical encoders measure the displacement of each motion stage with 20-μm resolution (Encoder Technology, Cottonwood, AZ). The actuators are ultrasonic motors (Shinsei travelling-wave USR60 USM) that contain no magnetic or ferrous components. The MRI compatibility of the robotic mechanism was evaluated in the open-MR scanner and found to produce no adverse effects. In fact, the robot created less field distortion than the body of the patient, as measured in reference [27].

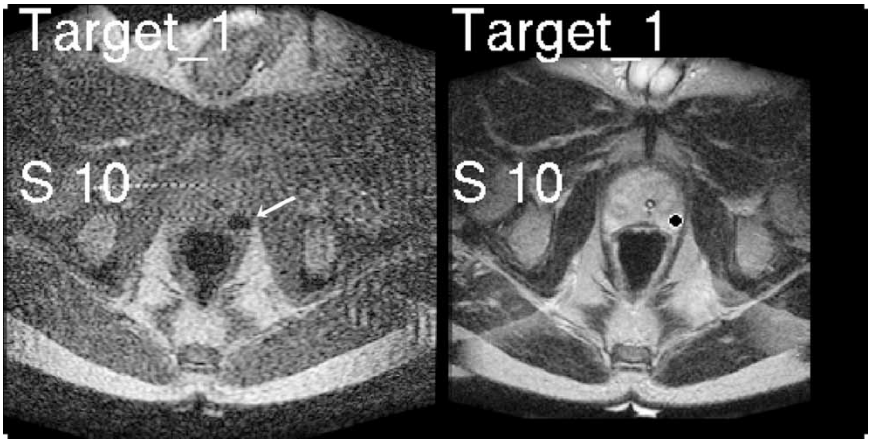

Figure 2. Images displayed to the physician during the procedure: FSE real-time image (left) showing needle artifact (arrow), and T2-weighted pre-procedure image (right) with a target marked in the peripheral zone. Distance to the target (superior 10 mm) is also displayed.

Figure 3. (a) GE Signa SP open-MRI scanner, with (b) integrated 5-DOF MR-compatible robot. The robot end-effector is equipped with an optical tracking marker (inset).

Calibration and control

Figure 1 illustrates the architecture of the system, which includes three major sub-systems, namely the MRI scanner, the planning interface, and the robotic mechanism with its associated controller. The planning sub-system – implemented within the 3D Slicer – also acts as a user interface for supervisory control of the robot during the intervention. The true position of the needle guide – measured by an optical tracker – is used to correct the position of the robot, as shown in Figure 4, where $\mathcal{J}(q)$ is an approximation of the manipulator Jacobian (long, flexible linkages introduce uncertainty), and X_e^I is the distance between the desired needle-guide pose (X^I) and that measured by the tracking system in the image-space ($X^{I'}$). X_e^R is the position error of the needle guide in the robot's frame of reference, while A is the transformation between image and robot coordinate frames. Δq is the resulting vector of joint displacements required to reposition the needle-guide and is computed as follows:

$$\Delta q = \mathcal{J}^{-1}(q)X_e^R = \mathcal{J}^{-1}(q)AX_e^I \qquad (1)$$

The matrix product $\mathcal{J}^{-1}A$ is calibrated prior to the procedure. The joint controller performs digital PID control of each joint independently, at a rate of 1000 Hz. The two feedback loops shown in Figure 4 are applied iteratively until X_e^I converges to within a predefined threshold. Once the needle guide is in position, MR scan plan coordinates are sent directly from the 3D Slicer to the scanning system's Real Time Control interface (see S_{RT} in Figure 1) for visualization of needle artifacts in real-time images (3- to 6-second image update).

Results of phantom experiments

Needle placement accuracy was quantified by targeting acrylic beads embedded in polyvinyl chloride (PVC) and gelatine tissue phantoms measuring approximately $9 \times 9 \times 11$ cm. The beads – each with a hole diameter of 3.5 mm – were embedded at depths of up to 9 cm from the inferior surface of the phantom. The tissue phantom was placed into a patient leg model, as shown in Figure 5a, and transferred into the MRI scanner in order to mimic the workspace available during the clinical procedure. Sterile draping was applied to both the patient model and the robot manipulator arms, as shown in Figure 5b. The phantom was scanned and the image volume imported into

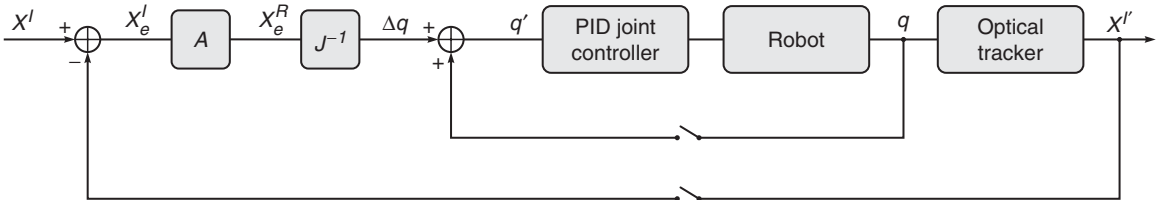

Figure 4. Robot control system block diagram.

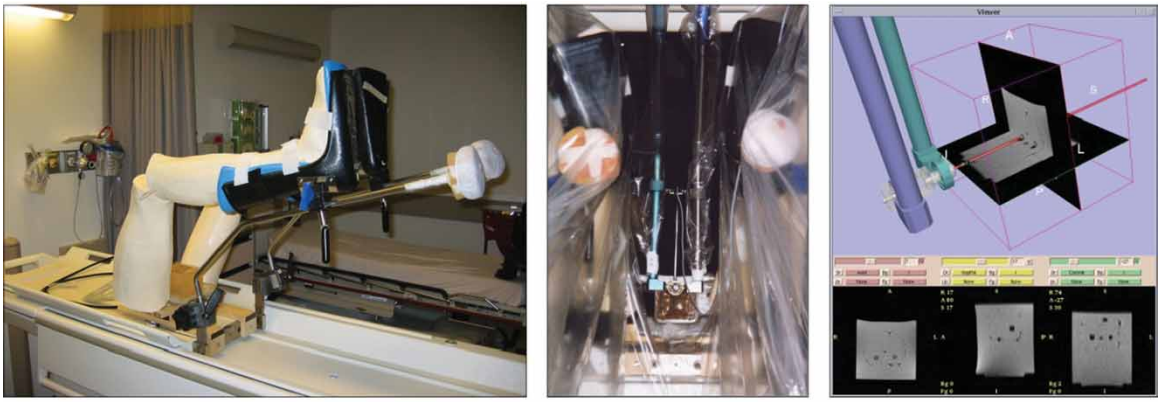

Figure 5. Phantom experiments: (a) scale models of legs and PVC prostate phantom with embedded targets; (b) patient model and robot placement inside the scanner with sterile draping; (c) needle trajectories are interactively specified in the planning environment. [Color version available online.]

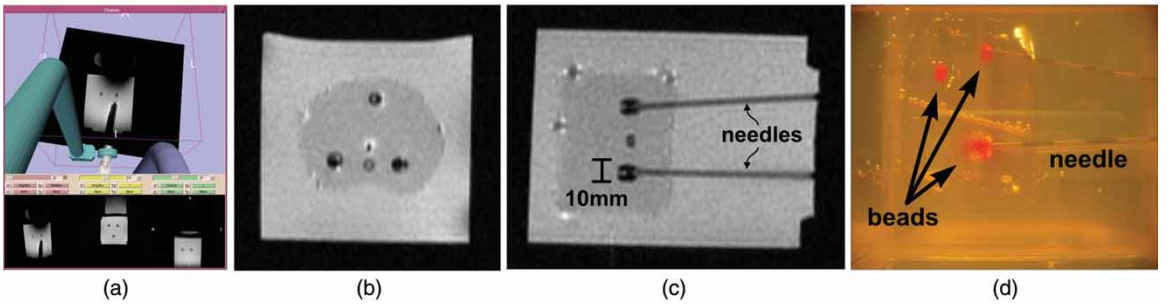

Figure 6. (a) Real-time image visualization in the Slicer interface during needle insertion; (b, c) MRI images of needle placement in the phantom; and (d) the target phantom. [Color version available online.]

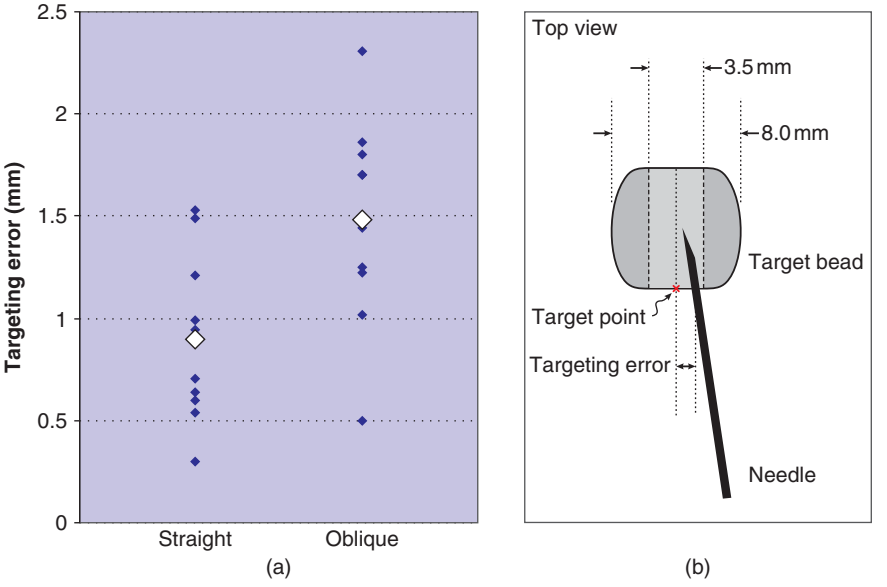

Figure 7. Needle placement accuracy measured during phantom experiments: (a) placement error for 10 straight needle trajectories and 11 oblique trajectories; (b) a schematic showing the top view and dimensions of the target beads and error measurement.

the 3D Slicer for planning and placement, as described in *System architecture* above and shown in Figure 5c.

In this study, we attempted to place 21 needles (18G MRI biopsy needles, E-Z-EM, Inc.) into the centers of 10 beads from a variety of different trajectory angles. Ten needle trajectories were chosen to lie straight along the inferior-superior axis, while the remaining 11 needles were placed at a variety of oblique angles. Target sites were selected from pre-procedural images of the phantom and were placed at the mouth of each bead, as illustrated in Figure 7(b). Placement accuracy was measured as the shortest lateral distance between the target point and the needle shaft; the depth of placement was not considered, since this is manually controlled by the physician. Needle visualization and placement are shown in Figure 6. Targeting errors are plotted in Figure 7a and summarized in Table 1.

Table 1. Measured needle placement accuracy.

Trajectory type	Average error [mm]	Standard deviation [mm]	RMS error [mm]
Straight needles ($N=10$)	0.89	0.41	0.98
Oblique needles ($N=11$)	1.5	0.48	1.6
All needles ($N=21$)	1.2	0.53	1.3

Discussion

We have developed an integrated planning system and a robotic assistant that acts as a dynamic needle

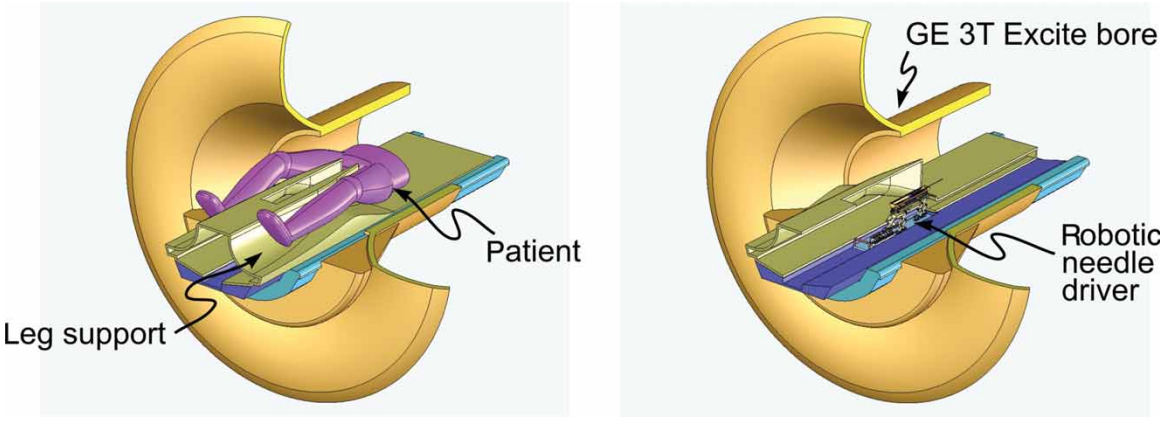

Figure 8. Closed-bore concept for MRI-guided needle placement. The patient's legs are placed on a leg support that provides a "tunnel" of access to the perineum. A compact robotic needle driver mechanism is placed into this tunnel as shown. [Color version available online.]

guide for percutaneous interventions in the prostate. This approach helps to simplify workflow by providing an interactive "point and click" trajectory-planning interface and an MRI-compatible robotic mechanism for precise, yet flexible needle placement for targeted interventions. In-scanner phantom tests have been performed in order to validate system performance and needle placement, and preparations are underway for a clinical trial.

In phantom experiments, the system consistently placed needles within 2 mm of their intended targets in a tissue phantom. System performance is dependent on accurate calibration between the optical tracker and the image coordinate space, as is also the case for all clinical cases undertaken in the MRT. An image-based registration and tracking approach would be preferable, and can be incorporated into our present system architecture. The advantage of such a visual servo approach is that the image and device coordinate systems are explicitly registered, as opposed to a "register and shoot" approach that is dependent on calibrated external sensors.

The system is based on a modular and extensible architecture that will be used as a testbed for the development of novel image-based navigation and visual servo techniques in open- and closed-bore MRI scanners, in order to be extended to other applications of MRI-guided percutaneous therapy in the future. The methodology developed in this work is now being transferred to a closed-bore magnet. A second-generation robotic needle placement mechanism was been designed to fit into a closed-bore magnet with the patient, while being controlled remotely by the physician. This concept is shown in Figure 8. The system will inherit the workflow, planning interface and software architecture developed in this work.

An important aim of this work is to develop techniques for validating new methods of image-based diagnosis and tumor identification, including multi-parametric and molecular imaging techniques, such as those based on Carbon-13 or other tracers. Whole-gland resection and analysis is not feasible for such validation; therefore, precise image-driven tissue sampling for subsequent histological analysis and correlation is needed.

Acknowledgments

This publication was made possible by NIH grants U41-RR019703 and P01-CA067165, as well as NSF ERC 9731748. Its contents are solely the responsibility of the authors and do not necessarily represent the official views of the NIH or the NSF. We would like to thank Janice Fairhurst for scanning assistance, Nicole Aucoin, Mike McKenna and Emese Balogh for assistance with Slicer programming, and Jordan Stephens for help with calibration.

References

1. D'Amico AV, Cormack RA, Tempany CM. MRI-guided diagnosis and treatment of prostate cancer. New England Journal of Medicine 2001;344(10):776–777.
2. Barnes AS, Haker SJ, Mulkern RV, So M, D'Amico AV, Tempany CM. Magnetic resonance spectroscopy-guided transperineal prostate biopsy and brachytherapy for recurrent prostate cancer. Urology 2005;66: 319.e13–1319.e15.

3. Padhani A, Gapinski C, Macvicar D, Parker C, Suckling J, Revell P, Leach M, Dearnaley D, Husband J. Dynamic contrast enhanced MRI of prostate cancer: Correlation with morphology and tumour stage, histological grade and PSA. Clin Radiol 2000;55:99–109.
4. Engelbrecht MR, Huisman HJ, Laheij RJ, Jager GJ, van Leenders GJ, Hulsbergen-Van Der Kaa CA, de la Rosette JJ, Blickman JG, Barentsz JO. Discrimination of prostate cancer from normal peripheral zone and central gland tissue by using dynamic contrast-enhanced MR imaging. Radiology 2003;229(1):248–254.
5. Kurhanewicz J, Vigneron D, Males R, Swanson M, Yu K, Hricak H. The prostate: MR imaging and spectroscopy. Present and future. Radiol Clin North Am 2000;38:115–138.
6. Haker S, Barnes A, Maier S, Tempany C, Mulkern R. Diffusion tensor imaging for prostate cancer detection: Preliminary results from a biopsy-based assessment. In: Proceedings of the International Society for Magnetic Resonance in Medicine: 13th Scientific Meeting and Exhibition, Miami, FL, May 2005.
7. So MJ, Haker S, Zou KH, Barnes AS, Cormack R, Richie JP, D'Amico AV, Tempany CM. Clinical evaluation of MR-guided prostate biopsy. In: Proceedings of the International Society for Magnetic Resonance in Medicine: 13th Scientific Meeting and Exhibition, Miami, FL, May 2005.
8. D'Amico AV, Tempany CM, Cormack RA, Hata N, Jinzaki M, Tuncali K, Weinstein M, Richie JP. Transperineal magnetic resonance image guided prostate biopsy. J Urol 2000;164(2):385–387.
9. DiMaio SP, Pieper S, Chinzei K, Hata N, Balogh E, Fichtinger G, Tempany CM, Kikinis R. Robot-assisted needle placement in open-MRI: System architecture, integration and validation. In: Proceedings of Medicine Meets Virtual Reality (MMVR13), Long Beach, CA, January 2005 Studies in Health Technology and Informatics 119. Amsterdam: IOS Press, 2005; 126–131
10. Jemal A. Cancer statistics, 2004. CA Cancer J Clin 2004;54(8):8–29.
11. Blasko JC, Mate T, Sylvester JE, Grimm PD, Cavanagh W. Brachytherapy for carcinoma of the prostate: Techniques, patient selection, and clinical outcomes. Semin Radiat Oncol 2002;12(1):81–94.
12. Cooperberg MR, Lubeck DP, Mehta SS, Meng MV, Carroll PR. The changing face of low-risk prostate cancer: Trends in clinical presentation and primary management. J Clin Oncol 2004;22(11):2141–2149.
13. Presti Jr JC. Prostate cancer: Assessment of risk using digital rectal examination, tumor grade, prostate-specific antigen, and systematic biopsy. Radiol Clin North Am 2000;38(1):49–58.
14. Terris MK, Wallen EM, Stamey TA. Comparison of mid-lobe versus lateral systematic sextant biopsies in detection of prostate cancer. Urol Int 1997;59:239–242.
15. Yu KK, Hricak H. Imaging prostate cancer. Radiol Clin North Am 2000;38(1):59–85.
16. Haker S, Warfield SK, Tempany CMC. Landmark-guided surface matching and volumetric warping for improved prostate biopsy targeting and guidance. In: Barillot C, Haynor DR, Hellier P, editors. Proceedings of the 7th International Conference on Medical Image Computing and Computer-Assisted Intervention (MICCAI 2004), Saint-Malo, France, September 2004. Part I. Lecture Notes in Computer Science 3216. Berlin: Springer; 2004. pp 853–861.
17. Chan I, Wells W, Mulkern R, Haker S, Zhang J, Zou K, Maier S, Tempany C. Detection of prostate cancer by integration of line-scan diffusion, T2-mapping and T2-weighted MR imaging; a multichannel statistical classifier. Med Phys 2003;30:2390–2398.
18. Shen D, Lao Z, Zeng J, Herskovits E, Fichtinger G, Davatzikos C. A statistical atlas of prostate cancer for optimal biopsy. In: Niessen WJ, Viergever MA, editors. Proceedings of the 4th International Conference on Medical Image Computing and Computer-Assisted Intervention (MICCAI 2001), Utrecht, The Netherlands, October 2001. Lecture Notes in Computer Science 2208. Berlin: Springer; 2001. pp 416–424.
19. D'Amico V, Cormack R, Tempany CM, Kumar S, Topulos G, Kooy HM, Coleman CN. Real-time magnetic resonance image-guided interstitial brachytherapy in the treatment of select patients with clinically localized prostate cancer. Int J Radiat Oncol 1998;42:507–515.
20. Zangos S, Eichler K, Engelmann K, Ahmed M, Dettmer S, Herzog C, Pegios W, Wetter A, Lehnert T, Mack MG, Vogl TJ. MR-guided transgluteal biopsies with an open low-field system in patients with clinically suspected prostate cancer: Technique and preliminary results. Eur Radiol 2005; 15(1):174–82.
21. Susil RC, Camphausen K, Choyke P, McVeigh ER, Gustafson GS, Ning H, Miller RW, Atalar E, Coleman CN, Ménard C. System for prostate brachytherapy and biopsy in a standard 1.5 T MRI scanner. Magnetic Resonance in Medicine 2004;52:683–6873.
22. Beyersdorff D, Winkel A, Hamm B, Lenk S, Loening SA, Taupitz M. MR imaging-guided prostate biopsy with a closed MR unit at 1.5 T: Initial results. Radiology 2005;234:576–581.
23. Hata N, Blumenfeld P, DiMaio SP, Haker SJ, Zou KH, Tempany CMC. Needle placement accuracy in MRI-guided prostate biopsy of prostate cancer. In: Proceedings of the International Society for Magnetic Resonance in Medicine; 14th Scientific Meeting and Exhibition, Seattle, WA, May 2006.
24. Masamune K, Kobayashi E, Masutani Y, Suzuki M, Dohi T, Iseki H, Takakura K. Development of an MRI-compatible needle insertion manipulator for stereotactic neurosurgery. J Image Guided Surg 1995;1(4):242–248.
25. Felden A, Vagner J, Hinz A, Fischer H, Pfleiderer SO, Reichenbach JR, Kaiser WA. ROBITOM – robot for biopsy and therapy of the mamma. Biomedical Technology 2002; 47:2–5.
26. Hempel E, Fischer H, Gumb L, Hohn T, Krause H, Voges U, Breitwieser H, Gutmann B, Durke J, Bock M, Melzer A. An MRI-compatible surgical robot for precise radiological interventions. Comput Aided Surg 2003;8(4):180–191.
27. Chinzei K, Hata N, Jolesz FA, Kikinis K. MRI compatible surgical assist robot: System integration and preliminary feasibility study. In: Delp SL, DiGioia AM, Jaramaz B, editors. Proceedings of the Third International Conference on Medical Image Computing and Computer-Assisted Intervention (MICCAI 2000), Pittsburgh, PA, October 2000. Lecture Notes in Computer Science 1935. Berlin: Springer; 2000. pp 921–930.
28. Krieger A, Susil RC, Menard C, Coleman JA, Fichtinger G, Atalar E, Whitcomb LL. Design of a novel MRI compatible manipulator for image guided prostate interventions. IEEE Trans Biomed Eng 2005;52:306–313.

29. Ganesh G, Gassert R, Burdet E, Bleule H. Dynamics and control of an MRI compatible master-slave system with hydrostatic transmission. In: Proceedings of the IEEE International Conference on Robotics and Automation (ICRA), New Orleans, LA, April 2004. pp 1288–1294.
30. Stoianovici D. Multi-imager compatible actuation principles in surgical robotics. Int J Med Robotics Comput Assist Surg 2005;1:86–100.
31. Hata N, Jinzaki M, Kacher D, Cormak R, Gering D, Nabavi A, Silverman SG, D'Amico AV, Kikinis R, Jolesz FA, Tempany CM. MRI imaging-guided prostate biopsy with surgical navigation software: device validation and feasibility. Radiology 2001;220(1):263.
32. Chinzei K, Kikinis R, Jolesz FA. MRI compatibility of mechatronic devices: Design criteria. In: Taylor C, Colchester A, editors. Proceedings of the Second International Conference on Medical Image Computing and Computer-Assisted Intervention (MICCAI 99), Cambridge, UK, October 1999. Lecture Notes in Computer Science 1679. Berlin: Springer; 1999. pp 1020–1030.
33. Chinzei K, Hata N, Jolesz F, Kikinis R. Surgical assist robot for the active navigation in the intraoperative MRI: Hardware design issues. In: Proceedings of the IEEE/RSJ International Conference on Intelligent Robots and Systems (IROS 2000), Takamatsu, Japan, October 2000. pp 727–732.